MoS2 for ultrafast all-optical switching and modulation of THz fano metaphotonic devices

Srivastava, Yogesh Kumar; Chaturvedi, Apoorva; Manjappa, Manukumara; Kumar, Abhishek; Dayal, Govind; Kloc, Christian; Singh, Ranjan

2017

https://hdl.handle.net/10356/138361

https://doi.org/10.1002/adom.201700762

MoS$_2$ for ultrafast all-optical switching and modulation of THz metaphotonic devices

Yogesh Kumar Srivastava[1,2,*], Apoorva Chaturvedi[3,*], Manukumara Manjappa[1,2], Abhishek Kumar[1,2], Govind Dayal[1,2], Christian Kloc[3], Ranjan Singh[1,2#]

[1]Division of Physics and Applied Physics, School of Physical and Mathematical Sciences, Nanyang Technological University, 21 Nanyang Link, Singapore 637371

[2]Center for Disruptive Photonic Technologies, The Photonics Institute, Nanyang Technological University, 50 Nanyang Avenue, Singapore 639798

[3]School of Materials Science and Engineering, Nanyang Technological University, Singapore, 639798

Corresponding author, E-mail: ranjans@ntu.edu.sg

* Equal contribution

Abstract:

In recent years, the stunning performance of transition metal dichalcogenides (TMDCs) has been utilized in the area of field effect transistors, integrated circuits, photodetectors, light generation and harvesting, valleytronics, and van der Waals (vdW) heterostructures. However, the optoelectronic application of TMDCs in realizing efficient, ultrafast metaphotonic devices in the terahertz part of the electromagnetic spectrum has remained unexplored. The most studied member of the TMDC family, i.e., MoS$_2$ shows an ultrafast carrier relaxation after photoexcitation with near-infrared femtosecond pulse of energy above the band gap. Here, we investigate the photoactive properties of MoS$_2$ to demonstrate an ultrasensitive active switching and modulation of the sharp Fano resonances in MoS$_2$ coated metamaterials

consisting of asymmetric split ring resonator arrays. Our results show all-optical switching and modulation of micron scale subwavelength Fano resonators could be achieved on a timescale of hundred picoseconds at moderate excitation pump fluences. The precise and active control of the MoS_2 based hybrid metaphotonic devices open up opportunities for the real-world technologies and realization of ultrafast switchable sensors, modulators, filters and nonlinear devices.

Introduction:

The perspective with regards to the layered materials (van der Waals solids) took a remarkable upturn with the isolation of monolayer graphene and a whole new regime of related low-dimensional material science, chemistry and physics.[1-3] Layered materials or van der Waals (vdW) solids are usually described by the presence of in-plane (intra-layer) covalent (strong) bonds and out-of-plane (inter-layer) vdW weak forces.[4] After the pioneering works in graphene, focus of the scientific community shifted towards the family of compounds known as transition metal dichalcogenides (TMDCs). This resulted partly due to the inability of a "zero" band-gap graphene and an urge to look for structurally similar and cheap materials with facile growth techniques to expand the catalogue of 2D materials.[5] TMDCs are MX_2- type compounds, where M is a transition element from groups IV, V and VI of the periodic table and X represents the chalcogen species S, Se and Te.[6] This family of compounds display an array of electronic properties ranging from semiconductor, semimetal, metal to superconductors depending on the choice of transition metal[7] and allows them to be the harbinger of future electronics and optoelectronic devices. Within the TMDCs, MoS_2 is the most investigated compound due to its availability in nature as a mineral (molybdenite).[8] Before this "renaissance" in the treatment of layered materials, MoS_2 was already studied for applications such as dry lubrication,[9-13] catalysis,[14-19] photovoltaics[20-23] and intercalation (batteries)[24-30] in the last five decades. Over the last few years, it assumed greater importance due to its unique and distinctive properties when it was discovered in few or monolayer form. For example, MoS_2 experiences a transition from an indirect band gap semiconductor in multi-layer form to direct band gap semiconductor in monolayer form in turn making it attractive for photo luminescent applications.[31] After initial synthesis and fabrication strategies were established for MoS_2, it has been employed in field effect transistors,[32] integrated and logic circuits,[22] optoelectronic devices such as photodetectors,[33] light

generation and harvesting,[34-37] valleytronics'[38] vdW heterostructres[39-40] and recently to mimic synaptics.[41] Although variety of studies has been performed on MoS$_2$, very limited fundamental studies have been done to explore the possibilities of MoS$_2$ based devices for ultrafast photonics. Here, in this work we exploit the photo-excitation properties of the MoS$_2$ to actively modulate the resonance properties of the metamaterial in a MoS$_2$-metamaterial hybrid device on an ultrafast time scale.

Metamaterials[44] are artificially structured composite arrays of sub-wavelength structures, which provides tremendous opportunities for controlling and manipulating electromagnetic light and have offered several unusual and novel phenomena such as negative refraction, super lenses, perfect absorption, invisibility cloaking, and much more.[45] The sub-wavelength size resonators are designed to yield a specific response to electric as well as the magnetic component of the incident light that provide unprecedented control over the light matter interactions. Typically, the high conductivity metals[46] are used for metamaterials in the terahertz part of the electromagnetic spectrum due to their low loss nature but they lack dynamism since the electromagnetic properties of metals are not very sensitive to external perturbations such as temperature and optical excitation. The dynamic control of the resonant properties in such metadevices in the real time is essential for the real-world device applications. The functional nature of the resonance response of metamaterials is achieved in several ways such as mechanical tuning of MEMS/NEMS[47-48] based structures or thermal, electrical, and optical tuning of structures based on phase-change materials such as semiconductors,[49-51] perovskites,[52-53] superconductors,[54] graphene[55] etc. The standard optoelectronic materials such as gallium arsenide, and silicon on sapphire have also shown exciting results in achieving actively tunable metamaterials but they require a more complex fabrication process.[49-51] The superconductor based metamaterials show highly tunable resonant response but their functionality is limited in real life applications as they fail to

operate at room temperature. The mechanical, thermal, and electrical switching responses are significantly slow while the optically tunable resonant devices based on dynamic materials show ultrafast switching, where the switching speed is governed by the lifetimes of the photo-excited carriers. The epitaxially grown silicon is highly used for realizing optically tunable resonant devices but the lifetime of the carriers falls in the range of milliseconds. Along with high modulation depth of the resonance properties, switching speed is equally important as it limits the application of the devices as modulators or switch. Hence, there is always an ongoing search for easily processable novel materials that could show high modulation at ultrafast time scales for new generation of photonic devices.

Here, we report the ultrafast relaxation of the bulk MoS_2 film prepared using the drop-casting method and integrate it with the subwavelength metaphotonic resonators to achieve dynamically controlled resonant properties of metadevices. Initial studies on the carrier dynamics of atomically thin MoS_2 revealed that the ultrafast dynamics and the relaxation time scale varies with increasing layer thickness. In the case of monolayer it falls in the range of few femtoseconds and for few layered MoS_2, it lies in the range of few picoseconds.[56-58] Since the exciton binding energies in bulk MoS_2 are close to the thermal energy at room temperature, the dynamics is almost entirely due to the free carriers rather than bound excitons which is further confirmed by the Drude-Smith conductivity behavior.[59] Drop casting of MoS_2 over planar metasurface offers great advantages in terms of cost effectiveness and simplification of the process to realize an active subwavelength metamaterial device as compared to other standard state-of-the-art materials that include complex fabrication processes including the clean room processing. The integration of MoS_2 on the metamaterials devices using drop casting method is highly economical, facile and fast process. We experimentally show the ultrafast, active photo-switching of Fano resonances in a MoS_2 coated Fano resonant metamaterial array. Fano resonances arise due to the interference

between a narrow discrete mode and broad continuum which results in the asymmetric line shape resonance.[60-63] The most striking feature of Fano resonances is the strong confinement of the electric fields in the resonator structure. The ultrafast response of MoS_2 coated Fano resonators pave the way for active meta-devices which have multifunctional applications in the lasing spaser,[64] ultrasensitive sensors,[65] and nonlinear applications,[66] and open up a new path in realizing the ultrafast photonic devices with enhanced functionalities in the terahertz, infrared and the optical region.

Results and Discussion:

To demonstrate active photoswitching of the Fano resonances in MoS_2 coated metamaterial, we fabricated an array of terahertz asymmetric split ring (TASR) structures on a THz transparent quartz substrate. **Figure 1 (a)** shows the graphical representation of the MoS_2 coated TASR metamaterial sample illuminated by a terahertz probe beam and femtosecond optical pump beam. Schematic of the unit cell describing the dimensions and the cross-sectional view of the device is shown in the inset of Figure 1(a). The TASR metamaterial sample was fabricated using the photolithography process. As a first step, a positive photoresist of thickness 1.5 micron was coated over the 1 mm thick cleaned z-cut quartz substrates and was pre-baked at a temperature of 105º C for 1 minute. The photoresist coated substrate was then exposed to UV light. The desired pattern was obtained by developing the pattern in the developer solution. The aluminum metal of thickness 200 nm was deposited on the substrates by thermal evaporation and the undesired aluminum was peeled off by soaking the samples in the acetone. The optical image of the small portion of fabricated TASR sample of size 10 mm x 10 mm is shown in Figure 1 (b). Later, the MoS_2 material was dispersed in ethanol and deposited over the metamaterial surface using an extremely facile drop casting technique. An identical MoS_2 film was coated on the quartz substrate to extract the optical constant of the MoS_2 film using terahertz time domain spectroscopy. To understand the

crystallinity of the drop-casted MoS_2, we performed X-ray diffraction analysis and obtained X-ray diffraction pattern as shown in **Figure 2 (a)**. Thin film X-ray diffraction analysis revealed highly crystalline MoS_2 phase with the observed peaks corresponding to the standard ICSD file # 95569 (shown in black line). Mostly peaks in (001) directions were observed on account of preferred orientation of the initially synthesized MoS_2 sample indicating the overall quality of the synthesized compounds. The morphological information of the film was obtained using the Atomic force microscopy (AFM) which revealed that the MoS_2 film has rms roughness of 280 nm and an average thickness of the film was ~400 nm. Figure 2 (b) and (c) depicts the 3D and 2D AFM image of the MoS_2 coated metamaterial sample.

The MoS_2 coated TASR sample with an asymmetry of $d = 10$ µm, was optically characterized by Optical-pump-Terahertz-probe (OPTP) measurements in a ZnTe crystal based terahertz time-domain spectroscopy (THz-TDS) system. The experimentally measured terahertz transmission spectra for various optical pump pulse powers are depicted in **Figure 3**. The Figure 3(a) represents the transmission spectrum of the TASR without MoS_2 layer, which shows sharp Fano line-shape resonance at 0.82 THz. When the MoS_2 film is coated on top of the metamaterial, it resulted in the red shift of the resonance position with slight reduction in transmission amplitude, as shown in Figure 3(b). The red shifting is due to the change in the gap capacitance of the TASR and the decrease in transmission amplitude is due to the semiconducting properties of the MoS_2 film which screens the fringing fields. When the pulsed near-infrared beam (100 fs with wavelength of 800 nm) with a pump power of 2 mW (fluence = 2.6 µJ/cm^2) was incident on the MoS_2 film, it photoexcited the charge carriers in the MoS_2 film which resulted in a small reduction in the amplitude of the Fano resonance (Figure 3(c)). The slight reduction in the transmission amplitude was due to low photo-excitation pump power. Upon further increase of the optical pump power to 10 mW (fluence = 12.7 µJ/cm^2), the density of the photoexcited carriers increased, which lead to a strong

7

reduction in the resonance amplitude, as shown in the Figure 3(d). When the pump power was increased from 10 mW (fluence = 12.7 µJ/cm²) to 100 mW (fluence = 127 µJ/cm²), the Fano resonance amplitude gradually reduced (Figure 3(e)) and eventually disappeared at an incident pump power of 200 mW (fluence = 254 µJ/cm²) (Figure 3(f)). We also defined the peak to peak transmission amplitude modulation depth of Fano resonance as $\left[(A_{\text{off}} - A_{\text{on}})/A_{\text{off}}\right] \times 100$ %, where A_{off} and A_{on}, respectively, stands for the transmission amplitudes during 'off' and 'on' state of optical pump and observed 9, 45, 96, and 100% modulation for the optical pump fluences 2.6, 12.7, 127, and 254 µJ/cm², respectively. The large modulation of the Fano resonance amplitude is observed due to the ultrasensitive photo-conducting properties of the MoS₂. As the incident pump power increased, the photoconductivity of the MoS₂ overlayer increased which shorted the capacitive gap of the TASR structure. The free carriers density due to the pump fleuence could be estimated using the relation $n_0 = \frac{\alpha \lambda f (1 - 10^{-OD})}{hc}$, where f and λ are the incident pump fluence and wavelength, respectively, α is the absorption coefficient of the MoS₂ at the incident wavelength, $(1 - 10^{-OD})$ is the fraction of pump light absorbed by the material.[67] *OD* is the optical density which is given by *OD*= 0.434α*t* for a material of thickness *t*. The estimated free carrier densities are 5.9 x 10¹⁷, 2.9 x 10¹⁸, 2.9 x 10¹⁹ and 5.8 x 10¹⁹ cm⁻³ for the pump fluences of 2.6, 12.7, 127 and 254 µJ/cm², respectively. We stress that the MoS₂ film was deposited by a robust and highly facile drop casting method with considerable roughness of the surface but the switching behavior outperforms devices fabricated with the state of the art materials in terms of the pump powers required to switch-off the resonance.

To further understand the photoexcitation behavior of the drop-casted MoS₂ film, we performed the OPTP measurements of an identical MoS₂ film drop-casted on the quartz substrate. By measuring the time-resolved, photo-induced THz conductivity in MoS₂ film, we

could monitor the charge-carrier dynamics. The differential transmission (-ΔT/T) of the terahertz pulse through an optically pumped MoS_2 film was used to extract the photoconductivity at different pump powers. For a thin film placed on a non-conducting and non-absorbing substrate, the complex transmission is given by[68]

$$T(\omega, t_p) = \frac{\tilde{T}_p(\omega, t_p)}{\tilde{T}_{Ref}(\omega)} = \frac{n+1}{n+1+Z_0\Delta\tilde{\sigma}(\omega, t_p)d} \quad (1)$$

where $\tilde{T}_P$ and $\tilde{T}_{Ref}$ are the transmission through the thin film and reference substrate, Z_0 is the free space impedance, d is the thickness of the thin film and n is the refractive index of the substrate in the terahertz wavelength range. From the above expression, the complex photoconductivity was calculated numerically as,

$$\Delta\tilde{\sigma}(\omega, t_p) = \frac{n+1}{Z_0 d}\left[\frac{1-T(\omega, t_p)}{T(\omega, t_p)}\right] \quad (2)$$

The extracted photoconductivity data for various pump powers are shown in **Figure 4**. The complex photoconductivity follows Drude-Smith behavior given by

$$\Delta\sigma(\omega) = \frac{\varepsilon_0\omega_p^2}{\Gamma - i\omega}\left[1 + \frac{C}{1 - i\omega/\Gamma}\right] \quad (3)$$

where the first term represents Drude conductivity and second term accounts for Smith correction.[69] The parameters ε_0, Γ and ω_p are vacuum permittivity, scattering time and plasma frequency respectively and C accounts for the backscattering which arises from trap and gain boundaries of sample and its value lies in the range of 0 to -1 where $C = 0$ denotes forward scattering and $C = -1$ signifies complete back scattering. The real and imaginary part of experimentally measured photoconductivity spectra were simultaneously fitted using Equation 3, and shown in Figure 4. The good agreement between measured data and fitted data imply that the response is entirely from the free charge carrier, where the backscattering comes from the surface inhomogeneity of the MoS_2 film.

9

In order to demonstrate the photo-induced switching in MoS_2 coated Fano resonant metamaterial, we also performed the numerical simulations using commercially available CST Microwave Studio software in the frequency domain, which solves Maxwell's equations by using Finite Integral techniques. In the simulation, quartz with dielectric constant of 3.75 was used as a substrate, aluminum metal with DC conductivity of 3.56 x 10^7 S/m was considered to design the metallic TASR array with a thin layer of MoS_2 coated on the top of the metamaterial unit cell. The permittivity of MoS_2 ($\varepsilon\sim12.25$) was extracted from the terahertz measurements. The transmission spectra for various photoconductivity has been simulated and shown in **Figure 5**. The simulations show similar trends of photo-switching which we observed in experiment (Figure 3). Further, we also simulated the electric field distribution in TASR at Fano resonance frequency. The electric field mainly concentrated at the capacitive gaps of the TASR (as shown in Figure 5 b) gives rise to a strong Fano resonance. The electric field strength was maximum for the sample without the MoS_2 (Figure 5 (b)). The enhanced photoconductivity of MoS_2 leads to the decrease in the capacitance which eventually causes the quenching of the Fano resonance. The annihilation of electric field at higher pump fluences signalled the switching-off of the Fano resonance in the metamaterial system.

Ultrafast charge carrier dynamics explains the electronic transport and optical properties of semiconductors. The fast relaxation of charge carriers excited above the band gap defines the switching time scale of materials for the ultrafast photonic applications. In bulk MoS_2, excitation of charge carrier by femtosecond laser created hot carriers in the conduction band that reached thermal equilibrium state in few picoseconds via both carrier-carrier and carrier-phonon scattering. In our case, we have used OPTP measurement scheme to investigate the ultrafast carrier dynamics in bulk MoS_2. **Figure 6** shows the transient dynamics of MoS_2 for different pump fluences ranging from 50 mW (63.5 μJ/cm^2) to 200 mW (254 μJ/cm^2). In

order to extract the lifetimes of fast and slow decay processes, all transients are fitted by bi-exponential decay function

$$y = y_0 + A_1 e^{(-\frac{(x-x_0)}{t_1})} + A_2 e^{(-\frac{(x-x_0)}{t_2})} \tag{4}$$

where t_1 reflects on the lifetime of fast process and t_2 is associated with the lifetime of slow decay process. The fast decay is due to the energy relaxation of the hot carriers until they reach thermal equilibrium, while the slow decay depicts the life time of the carriers.[58] Here it should be noted that the value of t_1 increased from 12 ps to 24 ps with pump fluences. This happens due to the hot phonon effect where large population generated by either higher lattice temperature or by larger photoexcitation fluences, along with slow phonon relaxation rate which prevents the carrier cooling by phonon emission.[70-71] Through our extraction using bi-exponential fitting, the slow carrier relaxation lifetimes falls in the range of hundreds of picoseconds. Here, we would like to highlight that drop casted MoS_2 coated active metamaterial resonant device could be switched-off and restored within sub-nanosecond time scales.

In conclusion, we have experimentally demonstrated that the drop-casted MoS_2 could be a perfect dynamic material for ultrafast, active photo-switching and modulation of the sub-wavelength Fano resonance based metaphotonic devices. Our results manifest the ultrafast switching of the Fano resonances on the time scale of 200 picoseconds in a MoS_2 hybrid metaphotonic devices. The drop casting of MoS_2 turns out to be a robust and facile method of deposition. The observed ultrafast and highly sensitive switching of the *E*-field confined in the gap of the resonators offer exciting opportunities for realizing ultrafast low energy subwavelength photonic devices. By integrating MoS_2 with metamaterial, an economical and robust active hybrid photonic devices can be realized with excellent multifunctional properties for nonlinear interactions, sensing, and lasing applications.

Methods:

1- Materials Synthesis

Initially high quality MoS_2 crystalline compound was synthesized via chemical vapor transport technique using $TeBr_4$ as a transport agent. As received molybdenum powder (99.9%, Alfa Aesar) and sulfur pieces (99.99%, Alfa Aesar) were vacuum sealed inside a quartz tube (ampoule) with an internal pressure of 10^{-5} torr. This sealed ampoule is subjected to a temperature profile of 950 ^{0}C at source zone and 900 ^{0}C at growth zone in a two-zone furnace for a period of 10 days. After the completion of the process, MoS_2 was carefully obtained for further characterization. For the ultrafast measurements, the obtained sample was dispersed in ethanol solvent and sonicated for 60 minutes. Later it was drop-casted on the required substrate (quartz and resonator) and simultaneously baked to evaporate the solvent. Here the choice of solvent and the power of sonication is moderate as the idea is to test the multi-layer MoS_2 sample response with facile preparation steps.

2- Materials Characterization

The deposited film via drop-cast method is characterized for phase purity via Shimadzu XRD-6000 (Cu-K_α radiation operated at 40 kV and 30 mA) configured in thin film mode. Further topographical and morphological information of the film was obtained using Piezoforce microscopy (PFM) [NT-MDT].

3- Optical pump-Terahertz probe Measurements

The terahertz transmission measurements were carried out using Optical-pump-Terahertz-probe (OPTP) setup that is based on ZnTe nonlinear THz generation and detection. Optical laser beam had a pulse width of ~ 100 fs, energy of 4 mJ/pulse at 800 nm with a 1 kHz repetition rate. The beam was split into two parts with one being used for pumping the ZnTe

crystal for THz generation-detection and the other part of the beam (800 nm, 1.55 eV) was used for optical excitation of MoS_2 layer. The photo-excitation pulse has higher photon energy than the band gap of the MoS_2 sample, which is about 1.2 eV. The optical pump beam has a beam diameter of approx. 6 mm, which is much larger than the focused terahertz beam spot size of nearly 3 mm at the sample position, providing uniform photo-excitation over the MoS_2 film. The time delay between optical-pump and terahertz probe pulses was controlled by using a translational stage and the delay is set to about 6 ps, where the photo-excited signal is the maximum. At this maximum pump signal, the terahertz scan was performed on the sample and the reference substrate and later in the post processing steps the spectrum through the sample ($E_S(\omega)$) is normalized to the reference substrate transmission spectra ($E_R(\omega)$) using the relation $|T(\omega)| = |E_S(\omega)|/|E_R(\omega)|$.

Acknowledgements:

References:

[1] K. S. Novoselov, A. K. Geim, S. V Morozov, D. Jiang, Y. Zhang, S. V Dubonos, I. V Grigorieva, and A. A. Firsov, *Science,* **2004**, *306*, 666.

[2] K. S. Novoselov, D. Jiang, F. Schedin, T. J. Booth, V. V Khotkevich, S. V Morozov, and A. K. Geim, *Proc. Natl. Acad. Sci. U. S. A.* **2005**, *102*, 10451.

[3] A. K. Geim, and K. S. Novoselov, *Nat Mater.* **2007**, *6*, 183.

[4] A. D. Yoffe, *Annu. Rev. Mater. Res.* **1973**, *3*, 147.

[5] P. R. Wallace, *Phys. Rev.* **1947**, *71*, 622.

[6] R. M. A. Lieth, J. C. J. M. Terhell, In *Preparation and Crystal Growth of Materials with Layered Structures*; Lieth, and R. M. A., Ed.; Springer Netherlands, 1977; pp. 141–223.

[7] R. Ganatra, and Q. Zhang, *ACS Nano* **2014**, *8*, 4074.

[8] D. Lembke, S. Bertolazzi, and A. Kis, *Acc. Chem. Res.* **2015**, *48*, 100.

[9] H. E. Sliney, *Tribol. Int.* **1982**, *15*, 303.

[10] M. R. Hilton, R. Bauer, S. V. Didziulis, M. T. Dugger, J. M. Keem, and J. Scholhamer, *Surf. Coatings Technol.* **1992**, *53*, 13.

[11] L. Rapoport, Y. Bilik, Y. Feldman, M. Homyonfer, S. R. Cohen, and R. Tenne, *Nature* **1997**, *387*, 791.

[12] M. Chhowalla, and G. A. Amaratunga, *Nature* **2000**, *407*, 164.

[13] C. Donnet, and A. Erdemir, *Tribol. Lett.* **2004**, *17*, 389.

[14] W. Jaegermann,and H. Tributsch, *Prog. Surf. Sci.* **1988**, *29*, 1.

[15] T. Y. Park, I.-S. Nam, and Y. G. Kim, *Ind. Eng. Chem. Res.* **1997**, *36*, 5246.

[16] M. Del Valle, J. Cruz-Reyes, M. Avalos-Borja, and S. Fuentes, *Catal. Lett.* **1998**, *54*, 59.

[17] P. Faye, E. Payen, and D. Bougeard, *Mol. Model. Annu.* **1999**, *5*, 63.

[18]   C. T. Tye, and K. J. Smith, *Top. Catal.* **2006**, *37*, 129.

[19]   Y. Yifei, S.-Y. Huang, Y. Li, S. N. Steinmann, W. Yang, and L. Cao, *Nano Lett.* **2014**, *14*, 553.

[20]   A. Jager-Waldau, M. C. Lux-Steiner, E. Bucher, In *Solid State Phenomema*; Strunk, H. P.; Werner, J. H.; Fortin, and B.; Bonnaud, O., Eds.; Trans Tech Publications, Switzerland, 1994; Vol. 37–38, pp. 479–484.

[21]   K. C. Kwon, C. Kim, Q. Van Le, S. Gim, J. Jeon, J. Y. Ham, J. Lee, H. W. Jang, S. Y. Kim, *ACS Nano,* **2015**, *9*, 4146.

[22]   D. Jariwala, V. K. Sangwan, L. J. Lauhon, T. J. Marks, and M. C. Hersam, *ACS Nano***2014**, *8*, 1102.

[23]   F. Bonaccorso, L. Colombo, G. Yu, M. Stoller, V. Tozzini, a. C. Ferrari, R. S. Ruoff, and V. Pellegrini, *Science (80-.).* **2015**, *347*, 1246501.

[24]   F. R. Gamble, J. H. Osiecki, and M. Cais, *Science (80-.).* **1971**, *174*, 493.

[25]   M. S. Whittingham, *Chemistry of intercalation compounds: Metal guests in chalcogenide hosts*; 1978; Vol. 12.

[26]   M. S. Whittingham, *Chem. Rev.* **2004**, *104*, 4271.

[27]   R. H. Friend, and A. D. Yoffe, *Adv. Phys.* **1987**, *36*, 1.

[28]   E. A. Mersegila, *Int. Rev. Phys. Chem.* **1983**, *3*, 177.

[29]   B. G. Silbernagel, *Mater. Sci. Eng.* **1977**, *31*, 281.

[30]   A. D. Yoffe, In *Physics and Chemistry of Electrons and Ions in Condensed Matter*; Acrivos, J. V.; Mott, N. F.; Yoffe, A. D., Eds.; Springer Netherlands, 1984; pp. 437–458.

[31]   K. F. Mak, C. Lee, J. Hone, J. Shan, and T. F. Heinz, *Phys. Rev. Lett.* **2010**, *105*, 136805.

[32]   B. Radisavljevic, a Radenovic, J. Brivio, V. Giacometti, and A. Kis, *Nat. Nanotechnol.* **2011**, *6*, 147.

[33]   O. Lopez-Sanchez, D. Lembke, M. Kayci, A. Radenovic, and A. Kis, *Nat. Nanotechnol.* **2013**, *8*, 497.

[34]   A. Splendiani, L. Sun, Y. Zhang, T. Li, J. Kim, C.-Y. Chim, G. Galli, and F. Wang, *Nano Lett.* **2010**, *10*, 1271.

[35]   Z. Yin, H. Li, H. Li, L. Jiang, Y. Shi, Y. Sun, G. Lu, Q. Zhang, X. Chen, and H. Zhang, *ACS Nano* **2012**, *6*, 74.

[36]   S. Mouri, Y. Miyauchi, and K. Matsuda, *Nano Lett.* **2013**, *13*, 5944.

[37]   M. Amani, D.-H. Lien, D. Kiriya, J. Xiao, A. Azcatl, J. Noh, S. R. Madhvapathy, R. Addou, S. KC, M. Dubey, K. Cho, R. M. Wallace, S.-C. Lee, J.-H. He, J. W. Ager, X. Zhang, E. Yablonovitch, and A. Javey, *Science (80-.).* **2015**, *350*, 1065.

[38]   K. F. Mak, K. L. McGill, J. Park, and P. L. McEuen, *Science (80-.).* **2014**, *344*, 1489.

[39]   A. K. Geim, and I. V Grigorieva, *Nature,* **2013**, *499*, 419.

[40]   H. Fang, C. Battaglia, C. Carraro, S. Nemsak, B. Ozdol, J. S. Kang, H. a Bechtel, S. B. Desai, F. Kronast, A. a Unal, G. Conti, C. Conlon, G. K. Palsson, M. C. Martin, A. M. Minor, C. S. Fadley, E. Yablonovitch, R. Maboudian, and A. Javey, *Proc. Natl. Acad. Sci. U. S. A.* **2014**, *111*, 6198.

[41]   A. J. Arnold, A. Razavieh, J. R. Nasr, D. S. Schulman, C. M. Eichfeld, and S. Das, *ACS Nano,* **2017**, *11*, 3110.

[42]   J. N. Coleman, M. Lotya, A. O'Neill, S. D. Bergin, P. J. King, U. Khan, K. Young, A. Gaucher, S. De, R. J. Smith, I. V Shvets, S. K. Arora, G. Stanton, H.-Y. Kim, K. Lee, G. T. Kim, G. S. Duesberg, T. Hallam, J. J. Boland, J. J. Wang, J. F. Donegan, J. C. Grunlan, G. Moriarty, A. Shmeliov, R. J. Nicholls, J. M. Perkins, E. M. Grieveson, K. Theuwissen, D. W. McComb, P. D. Nellist, and V. Nicolosi, *Science,* **2011**, *331*, 568.

[43]   V. Nicolosi, M. Chhowalla, M. G. Kanatzidis, M. S. Strano, and J. N. Coleman, *Science (80-.).* **2013**, *340*, 1226419.

[44]   J. B. Pendry, A. Holden, D. Robbins, and W. Stewart, *IEEE Trans. Microwave Theory Tech*, **1999**, *7*, 2075.

[45]   V. M. Shalaev, *Nature Photonics,* **2007***, 1*, 41-48.

[46]   Y. K. Srivastava, M. Manjappa, L. Cong, W. Cao, I. Al-Naib, W. Zhang, R. Singh, *Adv. Opt. Mater.* **2015**, *4*, 457.

[47]   H. Tao, A. C. Strikwerda, K. Fan, W. J. Padilla, X. Zhang, and R. D. Averitt, *Phys. Rev. Lett*. **2009**, 103, 147401.

[48]   P. Pitchappa, M. Manjappa, C. P. Ho, R. Singh, N. Singh, C. Lee, *Adv. Opt. Mater.*

2016, *4*, 541.

[49] W. J. Padilla, A. J. Taylor, C. Highstrete, M. Lee, and R. D. Averitt R. D., *Phys. Rev. Lett*. **2006**, 96, 107401.

[50] R. Yahiaoui, M. Manjappa, Y. K. Srivastava, and R. Singh , *Appl. Phys. Lett.*, **2017**, *111*, 021101.

[51] M. Manjappa, Y. K. Srivastava, L. Cong, I. Al-Naib, R. Singh, *Adv. Mater.* **2016,** *29(3)*, 1603355.

[52] M. Manjappa, Y. K. Srivastava, A. Solanki, A. Kumar, T. C. Sum, and R. Singh, *Adv. Mater.* , **2017,** *29*, 1605881.

[53]   L. Cong, Y. K. Srivastava, A. Solanki, T. C. Sum, and R. Singh, *ACSPhotonics*, **2017**, *4*, 1595.

[54]   R. Singh, N. Zheludev, *Nat. Photonics*, **2014**, *8*, 679.

[55] O. Li, Z. Tian, X. Zhang, R. Singh, L. Du, J. Gu, J. Han, and W. Zhang, *Nat. Commun.* **2015,** *6*, 7082.

[56]   H. Wang, C. Zhang, and F. Rana, *Nano Lett.*, **2015**, *15*, 339.

[57] R. Wang, B. A. Ruzicka, N. Kumar, M. Z. Bellus, H.-Y. Chiu, and H. Zhao, *Phy. Rev. B,* **2012**, *86*, 045406.

[58] N. Kumar, J. He, D. He, Y. Wang, and H. Zhao, *J. Appl. Phys.*, **2013**, *113,* 133702.

[59] T. Cheiwchanchamnangij, W. R. L. Lambrecht, Phy. Rev. B, **2012**, *85*, 205302.

[60] U. Fano, *Phys. Rev.* **1961**, *124*, 1866.

[61] B. luk'yanchuk, N. I. Zheludev, S. A. Maier, N. J. Halas, P. Nordlander, H. Giessen and C. T. Chong, *Nat. Mater.,* **2010**, 9, 707-715.

[62] V. A. Fedotov, M. Rose, S. L. Prosvirnin, N. Papasimakis, N. I. Zheludev, *Phys. Rev. Lett.* **2007**, *99*, 147401.

[63] R. Singh, I. A. I. Al-Naib, M. Koch, W. Zhang, *Opt. Express*, **2011**, *19*, 6312.

[64] N. I. Zheludev, S. L. Prosvirnin, N. Papasimakis, and V. A. Fedotov, *Nature Photonics,* **2008**, 2, 351-354.

[65]   M. Gupta, Y. K. Srivastava, M. Manjappa, R. Singh, *Appl. Phys. Lett.*, **2017**, *110*, 121108.

[66]   M. Kroner, A. O. Govorov, S. Remi, B. Biedermann, S. Seidl, A. Badolato, P. M. Petroff, W. Zhang, R. Barbour, B. D. Gerardot, R. J. Warburton, K. Karrai, *Nature,* **2008**, *451*, 311.

[67]   G. R. Yettapu, D. Talukdar, S. Sarkar, A. Swarnkar, A. Nag, P. Ghosh, and P. Mandal, *Nano Lett.*, **2016**, *16*, 4838.

[68]   P. U. Jepsen, D. G. Cooke, and M. Koch**,** *Laser Photonics Rev*., **2011**, *5 (1)*, 124.

[69]   R. Ulbricht, E. Hendry, J. Shan, T. F. Heinz, and M. Bonn, *Rev. Mod. Phys.,* **2011***, 83*, 543.

[70]   M. Seo, H. Yamaguchi, A. D. Mohite, S. B.-Tombet, J.-C. Blancon, S. Najmaei, P. M. Ajayan, J. Lou, A. J. Taylor, R. P. Prasankumar, *Sci. Rep.,* **2016***, 6,* 21601.

[71]   Z. Nie, R. Long, L. Sun, C.-C. Huang, J. Zhang, Q. Xiong, D. W. Hewak, Z. Shen, O. V. Prezhdo, and Z.-H. Loh, *ACS Nano*, **2014**, *8* (10), 10931.
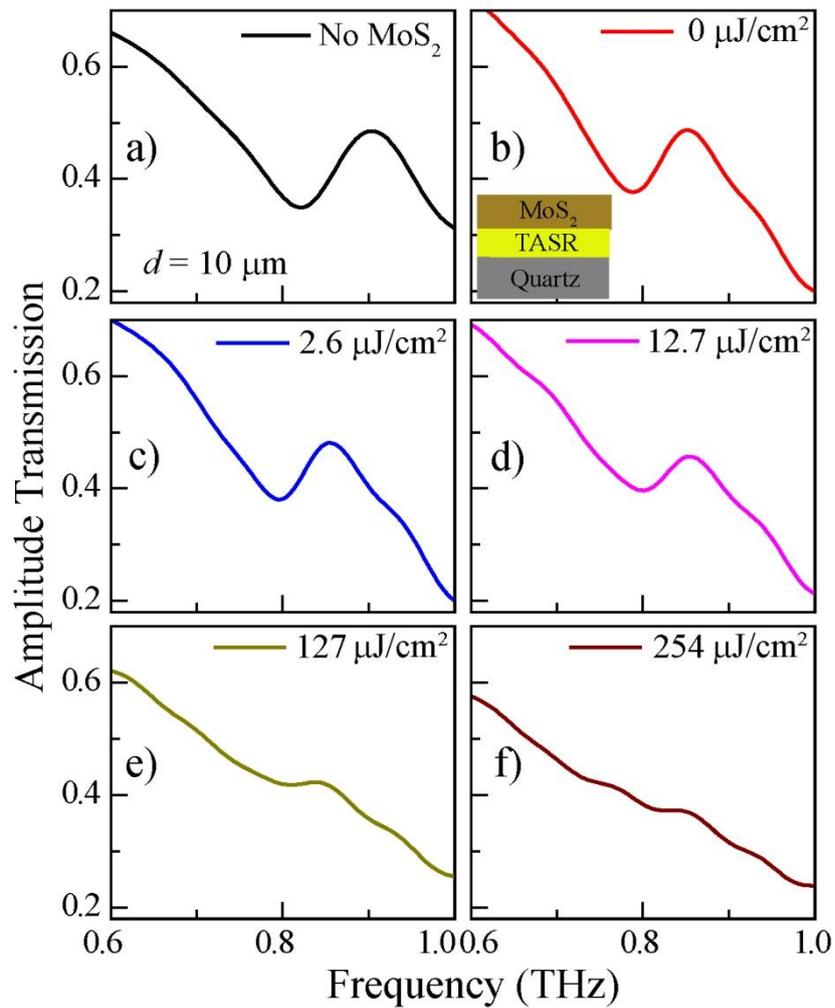
Figure 1
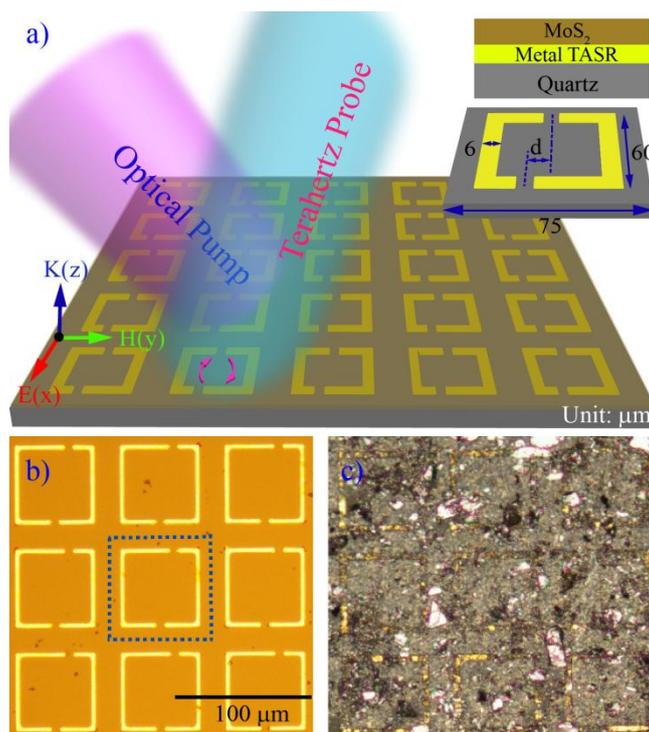
Figure 1: a) An artistic illustration of the MoS$_2$ drop casted on terahertz asymmetric split ring resonator (MoS$_2$-TASR) structure with the normal illumination of the optical pump and THz probe pulses. The inset represents the schematic of unit cell of the TASR highlighting the necessary structural dimensions in micron. Gaps in the TASR are 3 μm in size. Optical microscopy image of a small portion of the TASR metamaterial sample b) without MoS$_2$ and c) with drop casted MoS$_2$ layer.
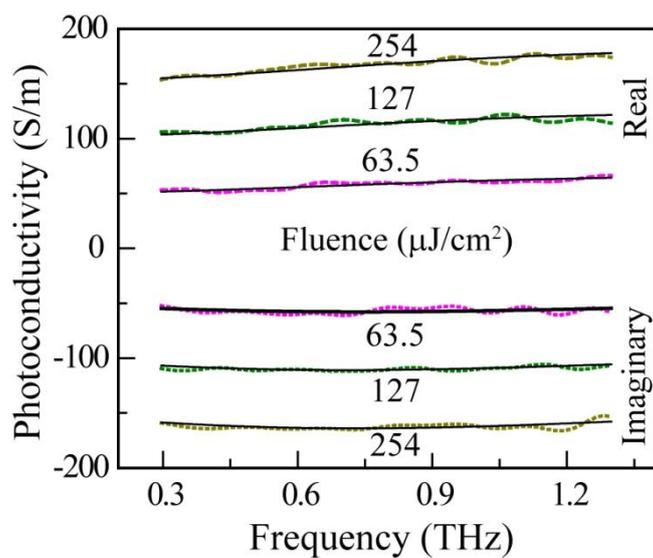
Figure 2
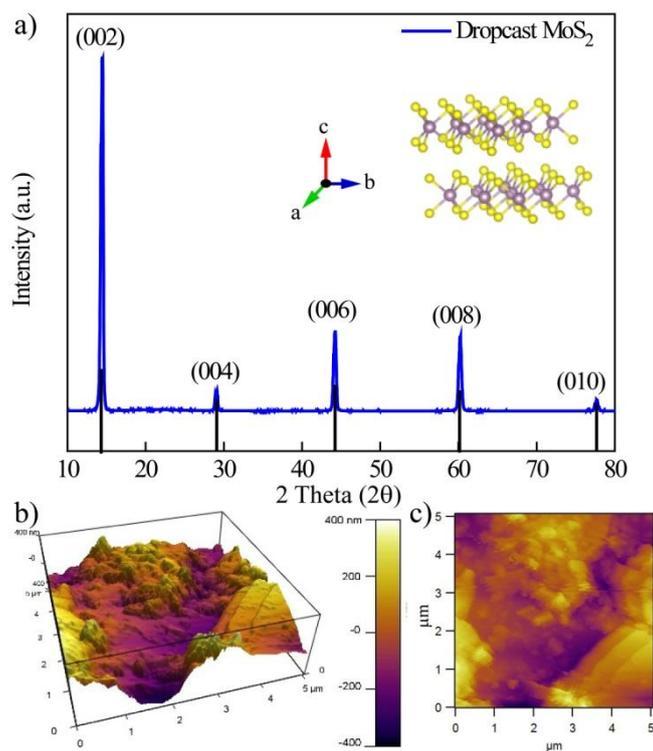
Figure 2: Measured X-ray diffraction (XRD) spectra of the drop casted MoS_2 over a quartz substrate. Black lines represent the simulated XRD pattern from the literature. (ICSD- 95569). (b)-(c) 3D and 2D Atomic force microscopy (AFM) image of the drop casted MoS_2 on the quartz substrate, respectively.
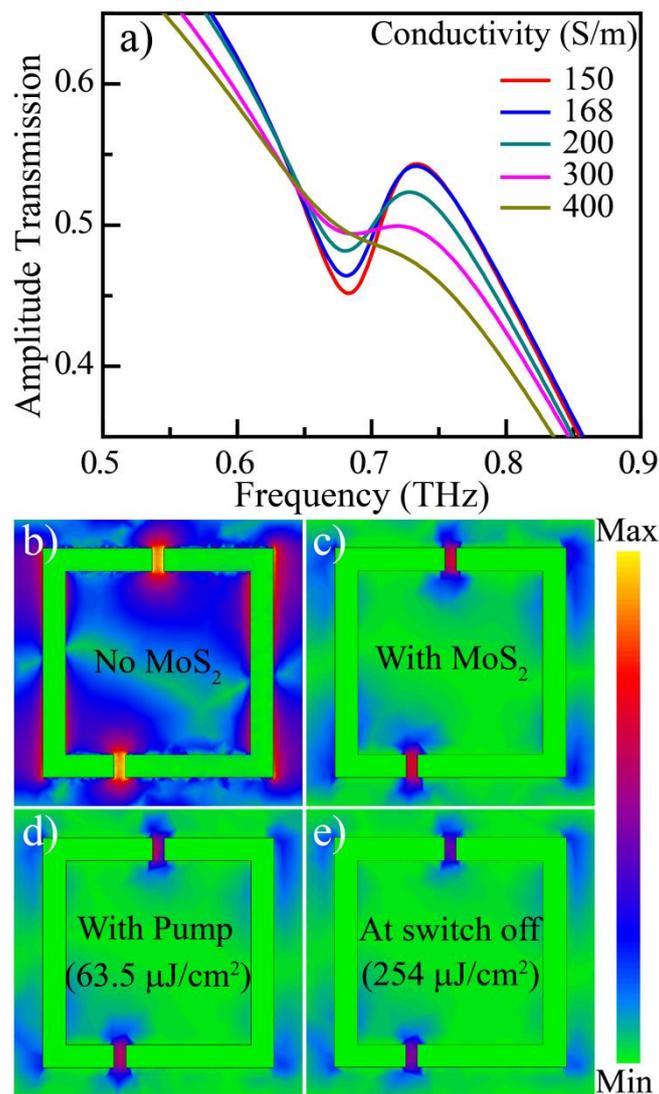
Figure 3

Figure 3: Experimentally measured terahertz transmission spectra of the fabricated metaphotonic device without MoS_2 (a), and with drop casted MoS_2 (b-f) layer at different optical pump fluences through OPTP measurements.
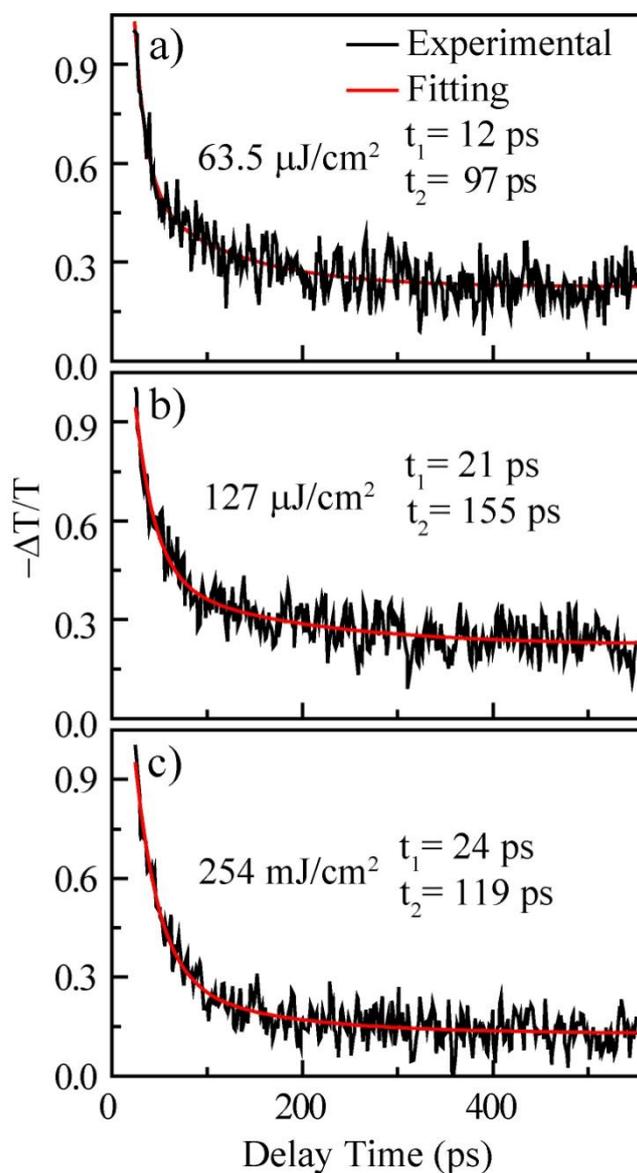
Figure 4

Figure 4: Experimentally measured (dotted) real and imaginary part of the photoconductivity spectra of drop casted MoS$_2$ film at varying excitation pump fluences. Solid lines represent the Drude-Smith fitting of the measured photoconductivity. The real and imaginary part of the conductivities are shifted vertically from each other for clarity.

Figure 5

Figure 5: a) Depicts numerically simulated amplitude transmission spectra by changing the photoconductivity of drop casted MoS_2 layer deposited on the TASR metamaterial structure. (b)-(e) Numerically calculated E-field distributions in the TASR metamaterial structure at the Fano resonance frequency for TASR without MoS_2, with MoS_2, and with optically pumped MoS_2 with low pump fluence ($63.5~\mu J/cm^2$) and switch-off of the Fano resonance with high pump fluence ($254~\mu J/cm^2$), respectively.

Figure 6

Figure 6: a)-c) Experimentally measured excitation dynamics (black line) of the drop casted MoS$_2$ film on a quartz substrate performed using the OPTP measurements at excitation pump fluence 63.5, 127 and 254 μJ/cm^2 along with the corresponding bi-exponential decay fitting (red line).